J. Fluid Mech. (1984), *vol.* 145, *pp.* 111–125
Printed in Great Britain

Source–sink flows of a stratified fluid in a rotating annulus

By JAE MIN HYUN
Department of Mechanical Engineering, Clarkson College of Technology, Potsdam, New York 13676

(Received 9 December 1982 and in revised form 6 March 1984)

We examine the steady axisymmetric source–sink flows of a stably stratified fluid in a rotating annulus, for which $S \sim O(1)$, $E \ll 1$. Numerical methods are used to integrate the unsteady Navier–Stokes equations to obtain the approximate steady solutions. Results on the radial and vertical structures of the flow and temperature-field details are presented. Specific comparisons of the relative sizes of the terms in the equations are conducted to reveal the balance of the dynamic effects. The profiles of the vorticity components are displayed. In the linear flow regime of a homogeneous fluid, the transport of fluid in the meridional plane takes place entirely via boundary layers. As stratification increases, the meridional flows are less concentrated in the boundary layers, and an appreciable portion of the meridional fluid transport is carried through the main body of fluid. The distinction between the sidewall layers and the interior becomes less clear. The flows in the main body of fluid develop vertical velocity shear, resulting in a thermal-wind relation. In the nonlinear case, the source sidewall layer thickens and the sink layer thins. As stratification increases, the meridional fluid transport through the main body of fluid is more pronounced than in the linear case. The balance of terms indicates that the bulk of the flow field is still characterized by the thermal-wind relation.

1. Introduction

In this paper we investigate the steady axisymmetric motions of a fluid confined in a rotating cylindrical annulus when the fluid is injected uniformly in the radial direction through the inner sidewall (source) and withdrawn through the outer sidewall (sink). The central axis of the annulus coincides with the vertical rotation vector, which is antiparallel to gravity. We consider the problems for which the aspect ratio of the annulus is $O(1)$ and the appropriately defined Ekman number E is minute.

Hide (1968) gave an informative account of the basic properties of such a flow system for a homogeneous fluid. This source–sink flow is particularly interesting in that the sidewall vertical boundary layers play a central role in determining the character of the interior flow (Barcilon 1968; Bennetts & Hocking 1973). The Ekman layers are present on the horizontal endwalls, but the layers are non-divergent; therefore the crucial Ekman suction mechanism, which controls the interior flow in situations like spin-up (see e.g. Wedemeyer 1964), is absent. The transport of fluid in the meridional plane takes place entirely via boundary layers; the fluid flows along the source sidewall layer toward the Ekman layers on the endwalls, and leaves the Ekman layers to flow toward the cylinder mid-depth in the sink sidewall layer. In the geostrophic interior there is no meridional motion, the (relative) azimuthal flows are in the opposite sense to the rotation, and the relative axial vorticity vanishes.

Bennetts & Jackson (1974, hereinafter referred to as BJ) performed a combined laboratory and numerical study of the rotating source–sink system of a homogeneous fluid over a range of the Rossby number. Their numerical results, which were checked against the experimental measurements of the azimuthal flows, provided detailed flow-field data in the sidewall layers as well as in the geostrophic interior. The numerical study of BJ demonstrated broad qualitative agreement with the theoretical predictions of Hide (1968). In the linear flow regime, BJ clearly showed the double structure of the sidewall boundary layer, the inner part being the $E^{\frac{1}{3}}$ layer superimposed on the outer $E^{\frac{1}{4}}$ layer. By displaying the radial profiles of the balance of terms in the equations of motion, BJ described the essential dynamical features that are present in the various parts of the flow field. They presented the results for the nonlinear case in which the inertial terms are no longer negligible. They showed the thickening of the source layer and the thinning of the sink layer in the nonlinear flow regime.

In this paper we propose to study the steady axisymmetric source–sink flows of a stably stratified fluid in a rotating annulus, much in line with the numerical approach taken by BJ for a homogeneous fluid. The modifications of the flow due to the introduction of stratification $S = O(1)$, where S is the stratification parameter (see §2), pose a suggestive model problem in which the dynamic constraints of both rotation and stratification are imposed in the sidewall boundary layers and in the geostrophic interior. It is anticipated that vertical motions in the sidewall layers will be inhibited owing to stable stratification. It will be shown that the radially injected mass flux can penetrate to a larger radial distance than for a homogeneous fluid. This implies that a substantial portion of the meridional fluid transport is carried through the main body of fluid. The vertical motions are spread out over the entire flow field, unlike the case of a homogeneous fluid, where vertical motions are confined to the narrow sidewall layers. It follows that, with increasing stratification, the sidewall layers themselves would become less distinct.

We have acquired comprehensive flow data for both the linear and nonlinear cases using a finite-difference numerical method. Numerical solutions were obtained for the unsteady flow of a stratified fluid, initially in a state of solid-body rotation, in response to an impulsively started radial mass injection–withdrawal at the sidewalls. Integration of the full Navier–Stokes equations was continued until the flow becomes approximately steady (see §3). Results on the radial and vertical structures of the flow and temperature fields in the approximate steady state are presented. Some specific comparisons of the relative sizes of the terms in the equations enabled us to observe the changes brought by the stratification and by the nonlinearities. Plots of the vorticity are also presented, which relate to the gradients of the flow. It is found that for a stratified fluid the dominant features in the main body of fluid are determined by the Coriolis effect and the buoyancy effect, resulting in a thermal-wind relation.

2. The numerical model

Consider a right-circular annulus, whose inner and outer radii are a and b respectively, and whose height is H, filled with a Boussinesq fluid having kinematic viscosity ν, thermal diffusivity κ and coefficient of volumetric expansion α. These physical properties of the fluid are assumed to be constant. The top and bottom endwalls are thermal conductors and are kept at constant temperatures to produce a stable stratification. The vertical temperature difference is ΔT over H. The sidewall boundaries are thermally insulated. The Froude number $\Omega^2 a^2/gH$ is much smaller than one.

The axisymmetric incompressible Navier–Stokes equations written for cylindrical coordinates (r, θ, z) rotating with angular speed Ω are

$$\frac{\partial u}{\partial t} = -\frac{1}{r}\frac{\partial}{\partial r}(ru^2) - \frac{\partial}{\partial z}(uw) - \frac{1}{\rho_0}\frac{\partial p}{\partial r} + \left(2\Omega + \frac{v}{r}\right)v + \nu\left(\nabla^2 u - \frac{u}{r^2}\right), \tag{1}$$

$$\frac{\partial v}{\partial t} = -\frac{1}{r}\frac{\partial}{\partial r}(ruv) - \frac{\partial}{\partial z}(vw) - \frac{vu}{r} - 2\Omega u + \nu\left(\nabla^2 v - \frac{v}{r^2}\right), \tag{2}$$

$$\frac{\partial w}{\partial t} = -\frac{1}{r}\frac{\partial}{\partial r}(ruw) - \frac{\partial}{\partial z}(w^2) - \frac{1}{\rho_0}\frac{\partial p}{\partial z} + \alpha g T + \nu\nabla^2 w, \tag{3}$$

$$\frac{\partial T}{\partial t} = -\frac{1}{r}\frac{\partial}{\partial r}(ruT) - \frac{\partial}{\partial z}(wT) + \kappa\nabla^2 T, \tag{4}$$

$$\frac{1}{r}\frac{\partial}{\partial r}(ru) + \frac{\partial w}{\partial z} = 0, \tag{5}$$

where

$$\nabla^2 = \frac{1}{r}\frac{\partial}{\partial r}r\frac{\partial}{\partial r} + \frac{\partial^2}{\partial z^2},$$

and (u, v, w) are the velocity components in the rotating frame, p the reduced pressure, T the temperature such that the full temperature equals $T_0 + T$, and ρ_0 and T_0 are respectively the reference values of density and temperature at the bottom endwall. The equation of state is

$$\rho = \rho_0(1 - \alpha T). \tag{6}$$

Since the problem is symmetric about the mid-depth plane $z = \frac{1}{2}H$, integration needs to be conducted for the bottom half of the cylinder, $0 \leqslant z \leqslant \frac{1}{2}H$, $a \leqslant r \leqslant b$, only.

The initial conditions for the fluid are

$$u = v = w = 0, \quad T = \frac{z\,\Delta T}{H} \quad \text{at} \quad t = 0. \tag{7}$$

The boundary conditions at the bottom endwall are

$$u = v = w = 0, \quad T = 0 \quad \text{at} \quad z = 0, \tag{8a}$$

and the symmetry conditions at the mid-depth plane are

$$\frac{\partial u}{\partial z} = \frac{\partial v}{\partial z} = w = 0, \quad T = \tfrac{1}{2}\Delta T \quad \text{at} \quad z = \tfrac{1}{2}H. \tag{8b}$$

The boundary conditions at the sidewalls are

$$u = u_{\mathrm{i}}, \quad v = w = 0, \quad \frac{\partial T}{\partial r} = 0 \quad \text{at} \quad r = a, \tag{9a}$$

$$u = \frac{u_{\mathrm{i}}\,a}{b}, \quad v = w = 0, \quad \frac{\partial T}{\partial r} = 0 \quad \text{at} \quad r = b. \tag{9b}$$

The sidewall boundary conditions (9*a*, *b*), give a uniform radial mass flux, but at the corner regions these are not compatible with the no-slip condition (8*a*) at the endwall. BJ specified a function $f(z)$, which gives a uniform flow over much of the sidewall but is designed to give a simple pattern of streamlines in the corner regions, in the sidewall boundary conditions. However, as BJ stated, there is no physical evidence

to support a particular choice of $f(z)$. BJ found that the disturbances that may arise from the incompatibility of the boundary conditions would be confined to a small corner area approximately $E^{\frac{1}{2}}$ by $E^{\frac{1}{3}}$. BJ also reported that any attempt to resolve the corner regions based on the pressure distribution leads to severe numerical complications. Based on these considerations and to avoid excessive numerical difficulties, we have decided to use (9) as the sidewall boundary conditions, disregarding the possible inconsistency in the small corner regions.

As a referee pointed out, the sidewall temperature boundary condition creates difficult conditions for a laboratory experiment. For the theoretical model this situation poses no serious difficulty. In this paper we consider a theoretical flow model that is amenable to mathematical treatment and that at the same time is useful in the comprehension of the essential dynamics.

Equations (1)–(6) and the initial and boundary conditions were finite-differenced on a staggered mesh. The grid was stretched in both the r- and z-directions to have adequate resolution of the boundary layers near the endwall and the sidewalls. The pressure was found from the Poisson equation obtained by taking the divergence of (1) and (3), which was solved by an ADI iterative approach. For details on the numerical techniques the reader is referred to Warn-Varnas *et al.* (1978). The reliability and accuracy of this numerical model have been verified previously for a variety of transient rotating and stratified flows by checking the model predictions against rotating laser-Doppler velocimeter (LDV) measurements in the laboratory spin-up experiments (Warn-Varnas *et al.* 1978; Hyun, Fowlis & Warn-Varnas 1982). All of these comparisons demonstrated excellent agreement between the results of this numerical model and the LDV measurements.

3. The computations

The numerical calculations were performed with the same geometrical and fluid parameters as those used by BJ:

$$a = 5.06 \text{ cm}, \quad b = 11.76 \text{ cm}, \quad H = 5.00 \text{ cm}, \quad \Omega = 0.25 \text{ rad/s}, \tag{10}$$

$$\nu = 1.00 \times 10^{-2} \text{ cm}^2/\text{s}, \quad \kappa = 1.46 \times 10^{-3} \text{ cm}^2/\text{s},$$

which give $E(\equiv \nu/2\Omega H^2) = 8.0 \times 10^{-4}$, $Pr(\equiv \nu/\kappa) = 6.85$.

BJ defined the Rossby number ϵ by $\epsilon = V_m/2\Omega H$, where V_m is the maximum azimuthal velocity. It should be noted, however, that V_m is a quantity that will only be known as part of the completed solution, rather than an input parameter that can be specified at the outset of the calculation. Since the motion is generated by radial mass injection–withdrawal, it appears to be more appropriate to link ϵ to the radial velocity at the sidewall (or the total volume flow rate passing through the container). For this purpose, we note that the azimuthal velocity scale is $E^{-\frac{1}{2}}$ times the meridional velocity scale (Hide 1968). Therefore we choose $V_0 \equiv E^{-\frac{1}{2}}u_i$ as the azimuthal velocity scale. We now define ϵ using V_0, i.e. $\epsilon = V_0/2\Omega H$. For the linear case, the value of u_i was set to be $u_i = 2.676 \times 10^{-5}$ cm/s, giving $\epsilon = 3.78 \times 10^{-4}$, which allowed us to reproduce very closely the homogeneous, linear flow regime treated by BJ. For the nonlinear case, as was done by BJ, the inflow rate was increased by a thousand times to $u_i = 2.676 \times 10^{-2}$ cm/s, giving $\epsilon = 0.378$. We kept the rotation rate constant so as not to alter the value of the Ekman number (Barcilon *et al.* 1975), and varied the value of $\alpha\Delta T$ to give three different values of the stratification parameter $S(\equiv (g\alpha\Delta T/H)^{\frac{1}{2}}/2\Omega) = 0$ (corresponding to a homogeneous fluid), 0.72, and 2.00.

Calculations were made using a 42×22 grid in the bottom half of the (r, z)-plane. The sensitivity of the results of this numerical model to grid size was tested by Warn-Varnas *et al.* (1978). The stretching of the grid enabled us to place about eight grid points in the Ekman layer. The time step used was $\Delta t = 0.00625$ s, which assured accuracy and satisfied the computational stability criteria described in Warn-Varnas *et al.* For a given set of parameters, the computer time to integrate the equations up to 200 s was approximately 4 h on a UNIVAC 1100 computer.

Some discussion is necessary about the nature of the approximate steady-state solutions that we are presenting in this paper. The solutions were obtained by integrating the unsteady equations, which arise in response to the impulsively started radial mass flux, to some finite time τ. In the case of homogeneous fluid ($S = 0$), as was reported by BJ, the approach to the steady-state solutions is approximately exponential for large times. BJ demonstrated that the variables are changing very slowly after about 3 e-folding spin-up times (see e.g. Wedemeyer 1964). For practical purposes, therefore, the integration was conducted to $\tau = 180$ s, at which time the solutions represent nearly 99% of the final-state conditions (see BJ). The solutions that we present for a stratified fluid are not as close to the strict steady-state solution as for a homogeneous fluid. The variables are still changing slowly with time, apparently governed by diffusive processes. Allen (1973) gave an illuminating discussion on the use of the approximate steady-state solutions. He considered the motions of a stratified fluid in a cylinder driven by the impulsively started differential rotation of the endwall; however, his discussion is equally valid for the problem in hand. The conclusion that emerges from Allen's discussion and a long-run test calculation (the case of $S = 0.72$ was integrated to 500 s) is that it is clearly unnecessary (and unpractical) to integrate the equations to the diffusive timescale, which is on the order of 2000 s for the present parameters, to depict the essential features of the steady-state conditions. The approximate steady-state solutions, which were obtained by terminating the integration at $\tau = 350$ s, would have small quantitative differences from the strict steady-state solutions. But, as Allen pointed out, these small remaining changes do not alter the qualitative character of the solutions, especially their relative nature.

The results of the computations are described in §§4 and 5. The discussion will be restricted to the flows in the bottom half of the annulus.

4. The linear case

In this section we present the results of the flow calculations for the linear case $\epsilon = 3.78 \times 10^{-4}$, for which the nonlinear terms are negligibly small.

4.1. *The velocity profiles*

The profiles of the azimuthal and radial velocities exhibit marked variations as the stratification is increased, as illustrated in figure 1. For a homogeneous fluid, v and u in the interior are uniform in the z-direction to a high degree of accuracy, a well-known phenomenon described by the Taylor–Proudman theorem. The radial velocity varies rapidly with r in the sidewall layers, which are scaled by $O(E^{\frac{1}{4}}H)$, and is very small (but not exactly zero because of the finite value of E) in the geostrophic interior. The profile of $-vr$ also displays rapid variations with r in the sidewall layers, but $-vr$ remains constant in the interior. As was documented by detailed comparisons by BJ, these profiles are qualitatively consistent with the predictions of the linear theory of Hide (1968).

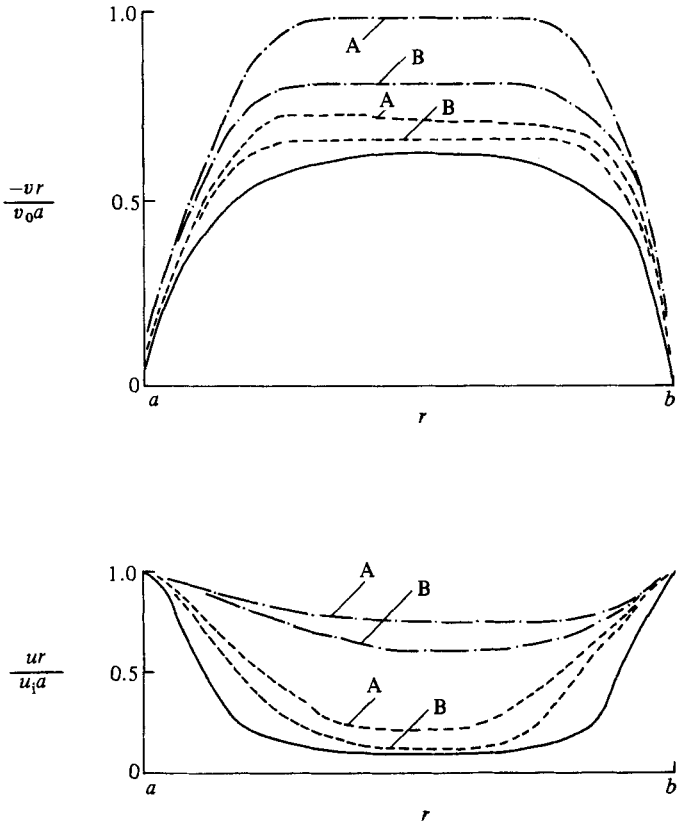

FIGURE 1. Profiles of $-vr$ and ur for $\epsilon = 3.78 \times 10^{-4}$. Label A denotes $z = 0.45H$, and label B denotes $z = 0.22H$. ——, $S = 0$; – – –, 0.72; — · —, 2.0.

As the stratification is introduced, the flow field undergoes changes in character. Before inspecting the flow details, it is informative to study the qualitative nature of the flows in the boundary layers and in the interior. This will provide physical insight into the dynamics involved in the changes brought by the stratification.

Following Pedlosky (1971), we split each field into its interior value (denoted by subscript I) plus a boundary-layer correction (denoted by subscript B). For example, for the azimuthal velocity $u = u_I + u_B$, where u_B vanishes outside the boundary layer. We recognize that the boundary layer fields are rapidly varying functions of r.

A consistent first approximation to the governing equations yields the following two useful relations between the boundary-layer variables (Pedlosky 1971):

$$\frac{\partial u_B}{\partial r} + \frac{\partial w_B}{\partial z} = 0, \tag{11}$$

$$2u_B = E\frac{\partial^2 v_B}{\partial \bar{r}^2}, \tag{12}$$

where $\bar{r} = r/H$.

Let us now consider the source sidewall boundary layer. As the stratification increases, vertical motions are suppressed, indicating that $\partial w_B/\partial z$ decreases in magnitude (pictures depicting the variations of w_B with depth will be given later). Equation (11) then shows that $\partial u_B/\partial r$ decreases in magnitude, i.e. the radial velocity

undergoes a smaller reduction in magnitude from its inflow velocity u_i at the sidewall. We deduce that, as stratification increases, the overall magnitude of the radial velocity in the boundary layer increases. It furthermore follows from (12) that the variation of v_B with r becomes more steep; this implies that, as stratification increases, the azimuthal velocity at the edge of the boundary layer increases in magnitude. A similar reasoning can be applied to the flow in the sink sidewall boundary layer.

In the interior, a cross-differentiation of the lowest-order r- and z-momentum equations for a stratified fluid produces

$$2\Omega \frac{\partial v_I}{\partial z} = \alpha g \frac{\partial T_I}{\partial r}, \tag{13}$$

which is the well-known thermal-wind relation. We observe that the descending fluid in the source layer is warmer and the ascending fluid in the sink layer is colder than the ambient fluid. Since the sidewalls of the annulus are thermally insulated, a negative radial temperature gradient is developed. As shown in (13), this radial temperature gradient supports the tilt in the profile of the azimuthal velocity. Because of this pronounced vertical shear of the azimuthal velocity, larger values of the radial velocity can be maintained in the interior.

In summary, the inhibition of vertical motions in the sidewall boundary layers due to stratification has far-reaching consequences on the flows in the boundary layers and in the interior. The numerical results illustrated in figure 1 verify the qualitative predictions that were described above. As stratification increases, the magnitude of the azimuthal velocity varies more steeply with r in the boundary layer and reaches a larger value in the interior. The radial velocities in the interior become substantial, implying that the radial mass flux can penetrate to a larger radial distance than for a homogeneous fluid. In the linear flow regime, these velocity profiles maintain near symmetry about the mid-radius $r = \frac{1}{2}(a+b)$ of the annulus. For a stratified fluid, the z-uniformity of u and v in the interior is no longer sustained; the flows of a stratified fluid can support vertical velocity shear.

Figure 2 shows the contour plots of v and the meridional stream function ψ. Here ψ is defined such that $u = -(1/r)\,\partial\psi/\partial z$ and $w = (1/r)\,\partial\psi/\partial r$. The top plots of figure 2 clearly show that for a homogeneous fluid the azimuthal velocity in the interior is uniform in the z-direction and that the meridional fluid transport takes place via boundary layers. For a stratified fluid (see the bottom plots of figure 2), the azimuthal velocity field supports vertical shear. The v-plot also shows that the Ekman layer is weak and the interior azimuthal velocities themselves approach smoothly the boundary conditions at the endwall. The ψ-plot shows that an appreciable portion of the meridional fluid transport is carried through the interior. In fact, as stratification increases, the distinction between the sidewall layers and the interior becomes unclear.

Figure 3 shows the profiles of the vertical velocity w at different vertical levels. For a homogeneous fluid (see figure 3*a*), w is negative in the source layer, zero in the interior, and positive in the sink layer. As the vertical position moves away from the mid-depth, the magnitudes of w in the sidewall layers increase to accommodate the increased meridional flow rate, while the thickness of the sidewall layers remain substantially unchanged. The suppression of vertical motions due to stratification is clearly seen in figure 3(*b*) (note the difference in scales used in the ordinates of figures 3*a* and 3*b*). As was stated earlier, figure 3(*b*) suggests that it is not possible to define clearly the sidewall layers. The vertical flows are generally toward the endwalls

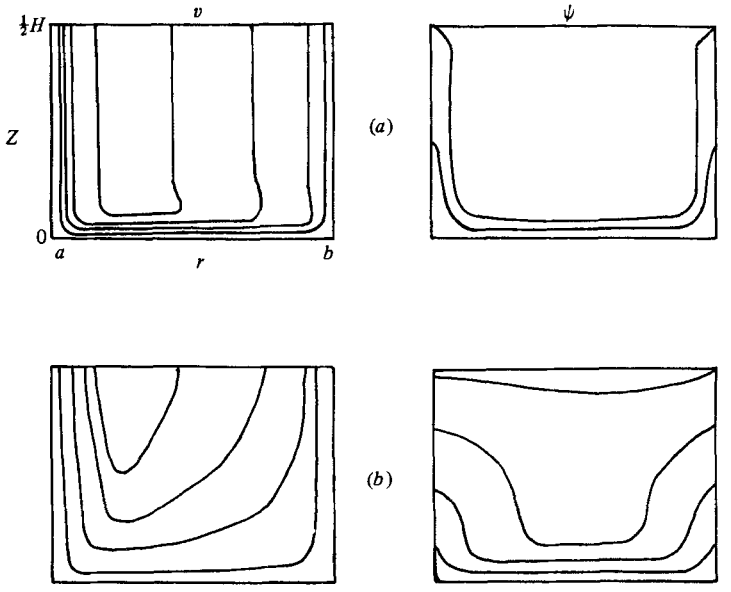

FIGURE 2. Contour plots for $\epsilon = 3.78 \times 10^{-4}$ of the azimuthal velocity v, and of the meridional stream function ψ. (*a*) $S = 0$; (*b*) $S = 2.0$. The specific values are: for $S = 0$, $v_{\min} = -0.46$, the contour interval $\Delta v = 0.10$, $\psi_{\max} = 1.63$, $\Delta\psi = 0.44$; for $S = 2.0$, $v_{\min} = -0.74$, $\Delta v = 0.16$, $\psi_{\max} = 1.20$, $\Delta\psi = 0.15$. v is expressed in units of V_0, and ψ in units of $\frac{1}{2}aHu_i$.

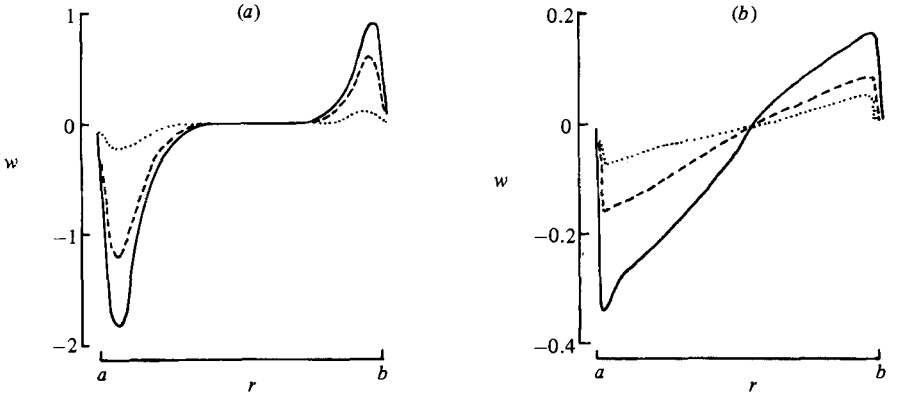

FIGURE 3. Profiles of the vertical velocity, expressed in units of u_i, for $\epsilon = 3.78 \times 10^{-4}$. (*a*) $S = 0$; (*b*) $S = 2$. ——, $z = 0.13H$; – – – –, $0.23H$; · · · · ·, $0.40H$.

(mid-depth) approximately in the half-meridional plane on the side of source (sink) sidewall. The variations of w with depth show a qualitatively similar trend to those for a homogeneous fluid.

4.2. *Relative size of terms*

Much can be learned about the balance of the dynamic effects by inspecting the relative sizes of the terms in the equations, often known as the diagnostic studies. The dominant flows are in the azimuthal direction, and it is informative to examine the terms in (2): the unsteady term is on the left-hand side of the equation, and the

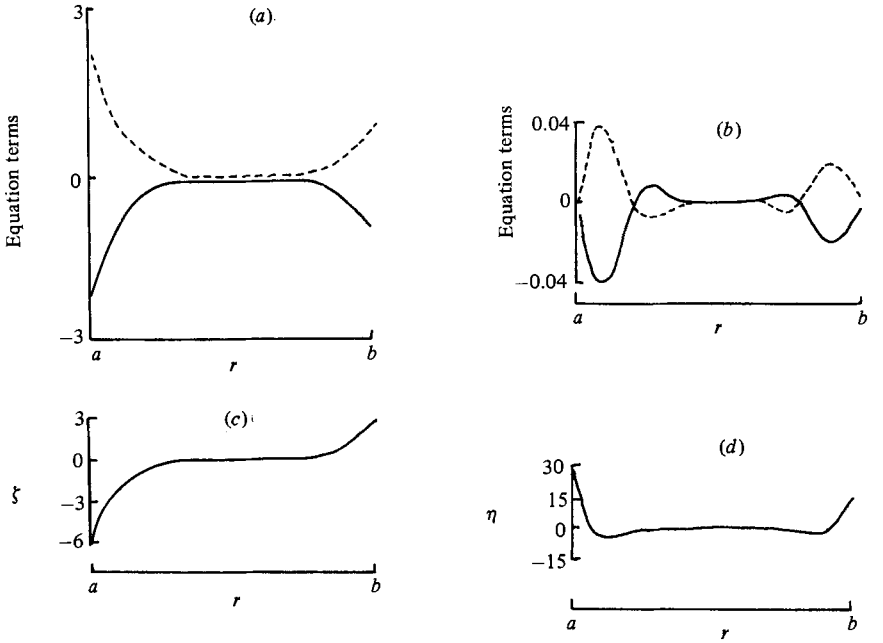

FIGURE 4. For $S = 0$, $\epsilon = 3.78 \times 10^{-4}$ at $z = 0.40H$. (*a*) Relative sizes of the terms in the v-equation (2), expressed in units of Ωu_1: ——, Coriolis term; – – –, viscous term. (*b*) Relative sizes of the terms in the η-equation (14), expressed in units of $V_0\Omega/H$: ——, Coriolis term; – – –, viscous term. (*c*) Axial vorticity ζ, expressed in units of V_0/a. (*d*) Azimuthal vorticity η, expressed in units of u_1/H.

terms on the right-hand side represent respectively the nonlinear advection in the r-direction, the nonlinear advection in the z-direction, the curvature effect (Warn-Varnas *et al.* 1978), the Coriolis acceleration, and the viscous diffusion. Information on the meridional flows can be combined into a single equation for the azimuthal component of vorticity $\eta(\equiv \partial u/\partial z - \partial w/\partial r)$:

$$\frac{\partial \eta}{\partial t} = -u\left(\frac{\partial \eta}{\partial r} - \frac{\eta}{r}\right) - w\frac{\partial \eta}{\partial z} + 2\frac{v}{r}\frac{\partial v}{\partial z} + 2\Omega\frac{\partial v}{\partial z} + \nu\left[\frac{\partial}{\partial r}\left(\frac{1}{r}\frac{\partial r\eta}{\partial r}\right) + \frac{\partial^2 \eta}{\partial z^2}\right] - \alpha g\frac{\partial T}{\partial r}. \tag{14}$$

The physical meaning of each term in (14) is similar to that of the corresponding term described earlier for (2), except for the last term in (14), which denotes the buoyancy (stratification) effect.

In all the diagnostic studies for the linear case, the nonlinear terms were several orders of magnitude smaller than the linear terms in the equations, and therefore the nonlinear terms will not be shown in the figures.

The results of the diagnostic studies for a homogeneous fluid are given in figure 4; figure 4(*a*) for the v-equation (2) and figure 4(*b*) for the η-equation (14), both of which were presented earlier by BJ. Figure 4(*c*) displays the profile of the axial component of vorticity $\zeta(\equiv (1/r)\partial(rv)/\partial r)$, and figure 4(*d*) shows the azimuthal component of vorticity η. These plots are included to illustrate the correspondence between the dynamic process and the behaviour of the vorticity. The results in figure 4 relate to the vertical level $z = 0.40H$, but figure 4 exemplifies typical situations in the regions away from the Ekman layer, since for a homogeneous fluid the solution is independent of z in the interior.

It is evident in figures 4(*a*, *b*) that the primary balance is between Coriolis

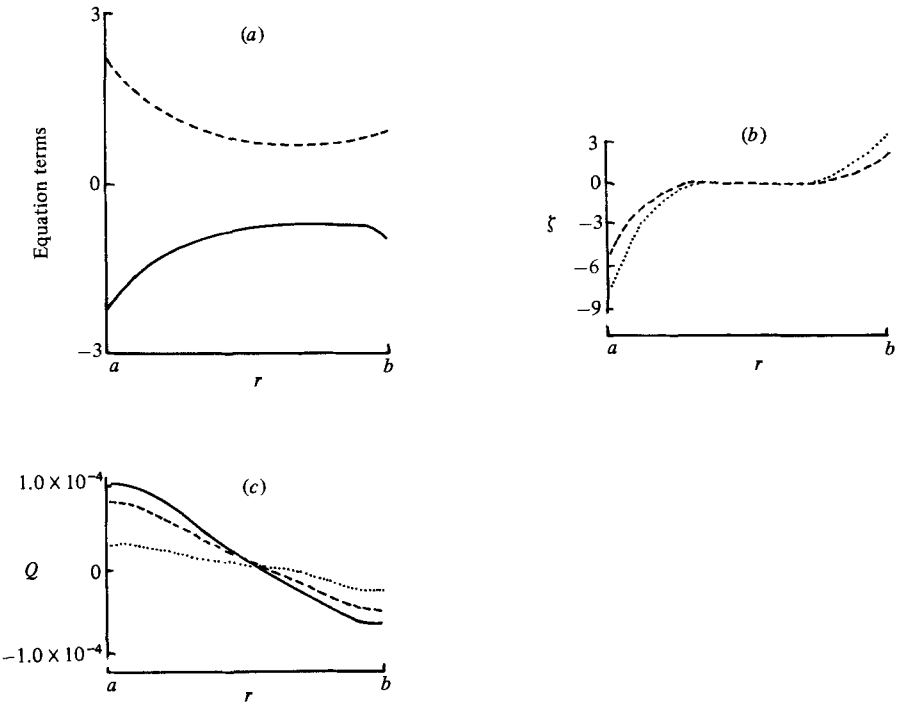

FIGURE 5. For $S = 2.0$, $\epsilon = 3.78 \times 10^{-4}$. (*a*) Relative sizes of the terms in the v-equation (2), expressed in units of Ωu_1, at $z = 0.23H$: ——, Coriolis term; – – –, viscous term. (*b*) Axial vorticity ζ, expressed in units of V_0/a: – – –, $z = 0.23H$; · · · · ·, $z = 0.40H$. (*c*) Temperature profile, $Q = T/\Delta T - z/H$: ——, $z = 0.13H$; – – –, $0.23H$; · · · · ·, $0.40H$.

acceleration and viscous diffusion. A further breakdown of the viscous term reveals that diffusion in the radial direction is predominant. It is also to be noted that the magnitudes of individual terms in the v-equation are vanishingly small in the interior. As was analysed by BJ, figure 4(*b*) depicts the double structure of the sidewall layers, which are composed of the inner $E^{\frac{1}{3}}$ layer within the $E^{\frac{1}{4}}$ layer. Figure 4(*c*) shows that, as can be inferred from the linear theory, ζ is negative in the source layer, zero in the interior, and positive in the sink layer. These numerical results indicate that ζ increases monotonically in the sidewall layers, unlike the predictions of the linear theory (compare figure 4(*c*) with figure 4(*b*) of Hide 1968). This difference is attributable to the neglect of the $E^{\frac{1}{3}}$ layer in the theory. Figure 4(*d*) shows that η is zero in the interior and non-zero in the sidewall layers. The double structure of the sidewall layers is also exhibited by the behaviour of non-zero η (see also figure 4*b*). A breakdown of η shows that $-\partial w/\partial r$ is the principal contributor.

The flow details for a stratified fluid are given in figures 5 and 6. A typical comparison of the terms in the v-equation is shown in figure 5(*a*). It is clearly demonstrated that the Coriolis term balances the viscous-diffusion term, which is qualitatively similar to the flow of a homogeneous fluid. However, both the Coriolis term and the viscous term for a stratified fluid are of sizable magnitude in the interior, reflecting the fact that u in the interior is significant for a stratified fluid (see figure 1). Furthermore, a breakdown of the viscous term shows that diffusion in the vertical direction is comparable to that in the radial direction, owing to the vertical velocity shear that is supported in the flow field.

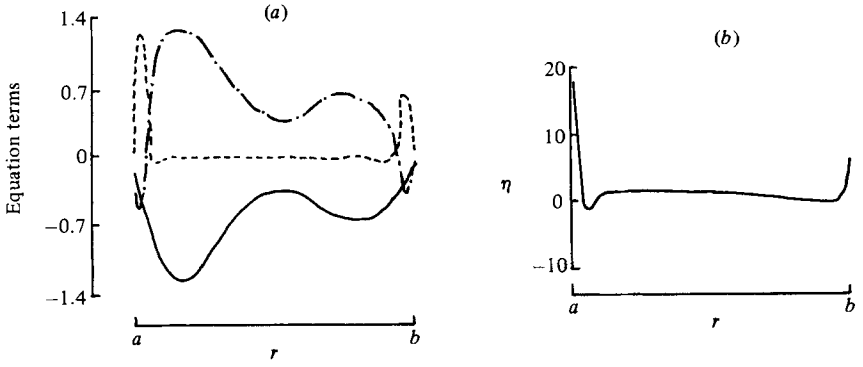

FIGURE 6. For $S = 2.0$, $\epsilon = 3.78 \times 10^{-4}$ at $z = 0.23H$. (*a*) Relative sizes of the terms in the η-equation (14), expressed in units of $V_0\Omega/H$: ——, Coriolis term; – – –, viscous term; —·—, buoyancy term. (*b*) Azimuthal vorticity η, expressed in units of u_i/H.

The profiles of the axial vorticity ζ depicted in figure 5(*b*) exhibit qualitative similarity to that of a homogeneous fluid (see figure 4*c*). As the vertical position varies, quantitative changes in ζ are seen in the regions where ζ is non-zero. This can also be deduced from the profiles of $-vr$ of a stratified fluid (see figure 1), which show a steeper variation of $-vr$ with r at a location closer to the mid-depth than at a location near the endwalls.

Figure 5(*c*) shows the temperature structure; Q represents the non-dimensional temperature deviation from the initial linear profile. The presence of negative temperature gradients in the interior is clearly seen.

Figure 6(*a*) illustrates the comparison of the terms in the η-equation (14) for a stratified fluid. It is apparent that the main body of flow field is characterized by a balance between the Coriolis effect and the buoyancy effect, i.e. $2\Omega\,\partial v/\partial z \approx \alpha g\,\partial T/\partial r$, which results in a thermal-wind relation. The vertical shear of the dominant azimuthal velocity is related to the radial temperature gradient. The effect of varying the vertical position causes quantitative changes only; the magnitude of the azimuthal velocity shear is smaller in the regions close to the mid-depth of the annulus than in the regions close to the endwalls, but the qualitative shape of these plots remains unchanged. A comparison of figures 4(*b*) and 6(*a*) points to the observation that, for a stratified fluid, the distinction between the sidewall layers and the interior is less clear.

Figure 6(*b*) shows that for a stratified fluid the maximum values of η are smaller than those for a homogeneous fluid. This reflects the fact that the meridional flows are less concentrated in the areas close to the sidewalls with increasing stratification (see figures 2*b*, 3*b*). The contributions from $-\partial w/\partial r$ and $\partial u/\partial z$ to η are of comparable magnitude. In the main body of flow field, the magnitudes of η are very small. The vertical variations of the η profiles (not shown here) indicate that the meridional flow gradients increase as the vertical position moves closer to the endwalls.

5. The nonlinear case

We now turn to the nonlinear case in which the inertial forces become important. The changes in the character of flows for a homogeneous fluid with larger Rossby numbers were analysed in detail by BJ. They demonstrated that in the nonlinear case

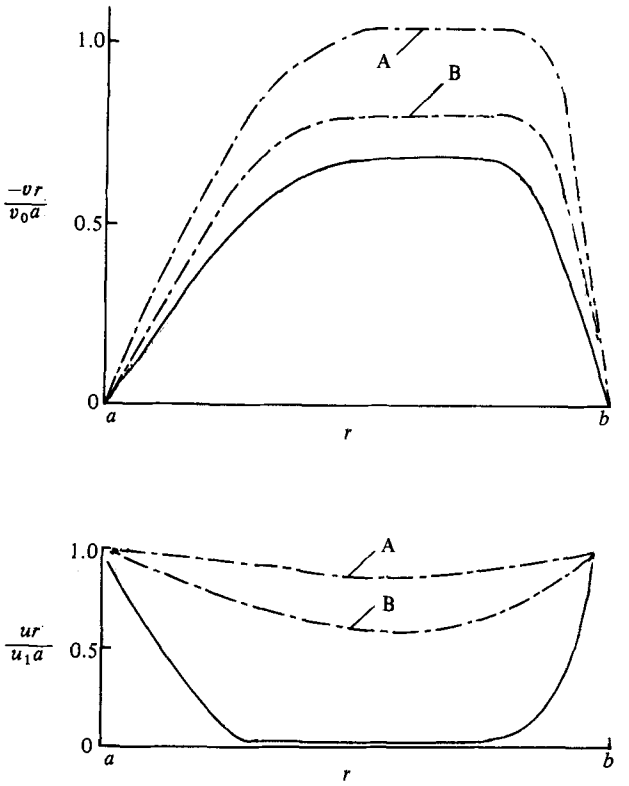

FIGURE 7. Same as in figure 1, except for $\epsilon = 0.378$: ——, $S = 0$; — · —, $S = 2.0$.

the source sidewall boundary layer thickens and the sink layer thins. BJ also noted the different distances that ur and $-vr$ require to approach their interior values. These qualitative properties in the nonlinear flow regime for a homogeneous fluid had been predicted by theory (Hide 1968; Bennetts & Hocking 1973).

The results of the computations using the Rossby number $\epsilon = 0.378$ for stratified fluids are presented in figures 7–11.

Comparisons of figures 1 and 7 clearly show the thickening of the source layer and the thinning of the sink layer. In particular, the $-vr$ plots in figure 7 indicate that it takes a considerably longer radial distance for $-vr$ to reach its interior values than for the linear case. Inspection of the contour plots shown in figure 8 reveals that the meridional transport through the main body of flow field for a stratified fluid is more pronounced in the nonlinear case.

The details of the nonlinear, homogeneous fluid flows are shown in figure 9. Figure 9(a) describes the balance of terms for the v-equation, and figure 9(b) shows the balance of terms for the η-equation. BJ also presented these two plots and discussed the physical implications in the nonlinear flow regime. For the v-equation, the primary balance in the source layer is between the geostrophic term and the nonlinear term. But, in the sink layer, the layer thins to allow the viscous effect to balance the other two. The profiles of the vorticity components, depicted in figures 9(c, d), are consistent with the flow behaviour in the sidewall layers discussed by BJ.

The results of the diagnostic studies for nonlinear stratified flows are presented in figures 10 and 11, corresponding to their linear counterparts shown in figures 5 and

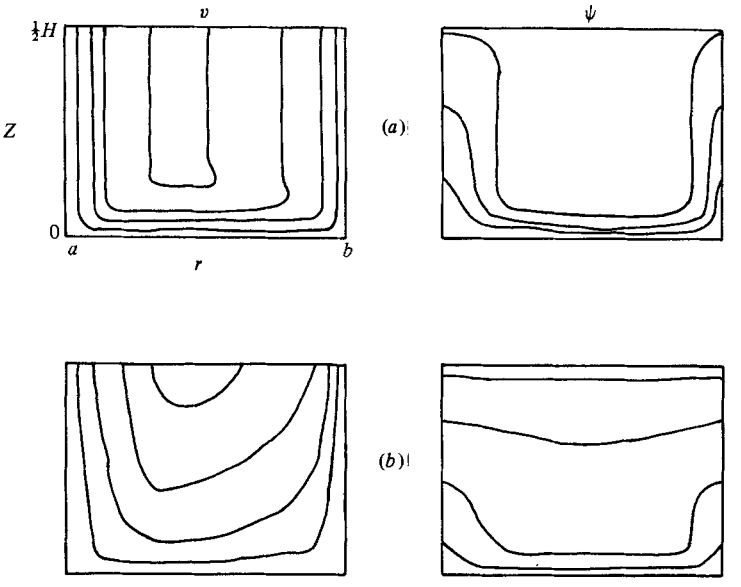

FIGURE 8. Same as in figure 2, except for $\epsilon = 0.378$. The specific values are: for $S = 0$, $v_{\min} = -0.46$, $\Delta v = 0.10$, $\psi_{\max} = 1.76$. $\Delta\psi = 0.44$; for $S = 2.0$, $v_{\min} = -0.67$, $\Delta v = 0.08$, $\psi_{\max} = 1.0$, $\Delta\psi = 0.30$.

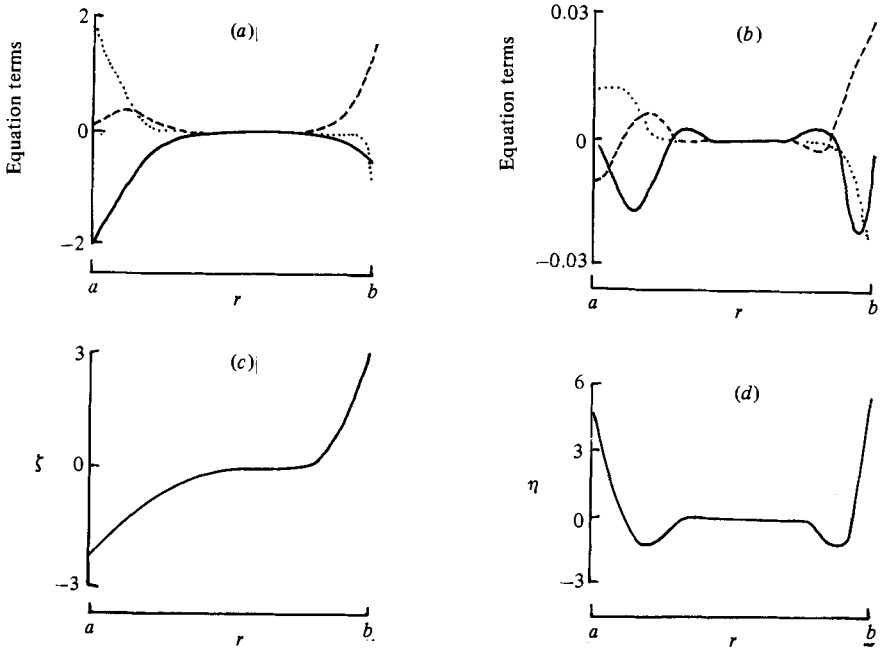

FIGURE 9. Same as in figure 4, except for $S = 0$, $\epsilon = 0.378$. In (*a*) and (*b*) ····· shows the nonlinear terms.

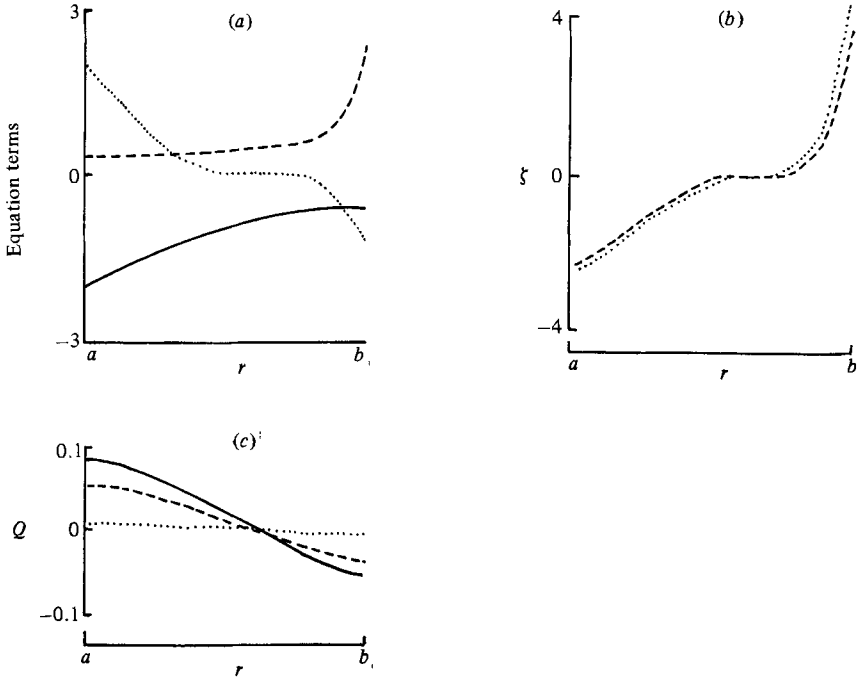

FIGURE 10. Same as in figure 5, except for $S = 2.0$, $\epsilon = 0.378$. In (a) ····· shows the nonlinear terms.

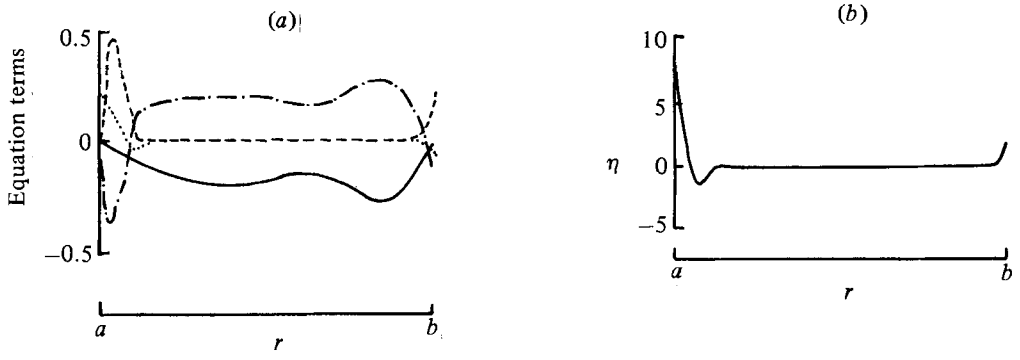

FIGURE 11. Same as in figure 6, except for $S = 2.0$, $\epsilon = 0.378$. In (a) ····· shows the nonlinear terms.

6 respectively. A comparison of figures 10(*a*) and 9(*a*) indicates that the profile of the nonlinear term changes little with the introduction of stratification. However, we notice in figure 10(*a*) that the magnitudes of the geostrophic term and the viscous term are appreciable in the bulk of the flow field (see figure 5*a*). The profiles of the axial vorticity (figure 10*b*) and of the temperature structure (figure 10*c*) are qualitatively similar to those for the linear case (see figures 5*b*, *c*).

The balance of terms for the η-equation for nonlinear, stratified flows is shown in figure 11(*a*). It is important to recognize that for the value of the Rossby number used in this study, $\epsilon = 0.378$, the main body of the flow field is still characterized by the thermal-wind relation. The nonlinear term and the viscous term are significant only in the regions very close to the sidewalls.

6. Conclusions

Numerical methods were used to obtain the approximate steady solutions for source–sink flows of a stratified fluid in a rotating annulus. The effect of stratification inhibits vertical motions in the sidewall layers, and consequently the radial mass flux can penetrate to a larger radial distance than for a homogeneous fluid. The flows in the main body of fluid develop vertical velocity shear that is balanced by the radial temperature gradient, resulting in a thermal-wind relation. With increasing stratification, the meridional flows are less concentrated in the boundary layers. Thus an appreciable portion of the meridional fluid transport is carried through the main body of fluid. As the Rossby number increases, the character of flow changes owing to the nonlinearities. For the nonlinear case, the source boundary layer thickens and the sink layer thins. Different force balances are sustained in these two layers in the nonlinear flow regime. As the stratification increases in the nonlinear flow regime, the meridional transport of fluid through the main body of fluid is more pronounced. Comparisons of the dynamic effects reveal that the main body of fluid still characterized by the thermal wind relation.

For a homogeneous fluid, the axial vorticity is zero in the interior and non-zero in the sidewall layers, but its variation with r is monotonic. The axial-vorticity profile for a stratified fluid is qualitatively similar to that for a homogeneous fluid. The merging of the sidewall layers and the interior leads to a qualitatively different pattern of vertical velocity profiles for a stratified fluid.

For a homogeneous fluid, the rapid variation of w with r in the sidewall layers is the primary contributor to the azimuthal component of vorticity. For a stratified fluid, the contribution from $\partial u/\partial z$ is comparable to that of $\partial w/\partial r$ in making up the azimuthal component of vorticity.

Appreciation is extended to the referees whose comments led to improvements in the paper. Dr William Fowlis of NASA Marshall Space Flight Center has provided many helpful comments on an earlier version of the manuscript.

REFERENCES

ALLEN, J. S. 1973 Upwelling of a stratified fluid in a rotating annulus: steady state. Part 2. Numerical solutions. *J. Fluid Mech.* **59**, 337–368.

BARCILON, V. 1968 Stewartson layers in transient rotating fluid flows. *J. Fluid Mech.* **33**, 815–825.

BARCILON, A., LAU, J., PIACSEK, S. & WARN-VARNAS, A. 1975 Numerical experiments on stratified spin-up. *Geophys. Fluid Dyn.* **7**, 29–42.

BENNETTS, D. A. & HOCKING, L. M. 1973 On nonlinear Ekman and Stewartson layers in a rotating fluid. *Proc. R. Soc. Lond.* A **333**, 469–489.

BENNETTS, D. A. & JACKSON, W. D. N. 1974 Source–sink flows in a rotating annulus: a combined laboratory and numerical study. *J. Fluid Mech.* **66**, 689–705.

HIDE, R. 1968 On source–sink flows in a rotating fluid. *J. Fluid Mech.* **32**, 737–764.

HYUN, J. M., FOWLIS, W. W. & WARN-VARNAS, A. 1982 Numerical solutions for the spin-up of a stratified fluid. *J. Fluid Mech.* **117**, 71–90.

PEDLOSKY, J. 1971 Geophysical fluid dynamics. In *Mathematical Problems in the Geophysical Sciences* (ed. W. H. Reid). American Mathematical Society.

WARN-VARNAS, A., FOWLIS, W. W., PIACSEK, S. & LEE, S. M. 1978 Numerical solution and laser-Doppler measurements of spin-up. *J. Fluid Mech.* **85**, 609–639.

WEDEMEYER, E. H. 1964 The unsteady flow within a spinning cylinder. *J. Fluid Mech.* **20**, 383–399.